[Cancer Biology & Therapy 6:3, e1-7, EPUB Ahead of Print: http://www.landesbioscience.com/journals/cbt/abstract.php?id=4019; March 2007]; ©2007 Landes Bioscience

Research Paper

Differentiation of Vascular and Non-Vascular Skin Spectral Signatures Using In Vivo Hyperspectral Radiometric Imaging

Implications for Monitoring Angiogenesis

Paul C. Tumeh[1]
Jeremy M. Lerner[2]
David T. Dicker[1]
Wafik S. El-Deiry[1,*]

[1]Laboratory of Molecular Oncology and Cell Cycle Regulation; Departments of Medicine (Hematology/Oncology), Genetics, Pharmacology, The Institute for Translational Medicine and Therapeutics, and the Abramson Comprehensive Cancer Center; University of Pennsylvania School of Medicine; Philadelphia, Pennsylvania USA

[2]Lightform, Inc.; Hillsborough, New Jersey USA

*Correspondence to: Wafik S. El-Deiry; University of Pennsylvania; 415 Curie Blvd.; Philadelphia, Pennsylvania USA; Tel.: 215.898.9015; Fax: 215.573.9139; Email: wafik@mail.med.upenn.edu

Original manuscript submitted: 02/16/07
Manuscript accepted: 02/16/07

This manuscript has been published online, prior to printing for Cancer Biology & Therapy, Volume 6, Issue 3. Definitive page numbers have not been assigned. The current citation is: Cancer Biol Ther 2007; 6(3):
http://www.landesbioscience.com/journals/cc/abstract.php?id=4019
Once the issue is complete and page numbers have been assigned, the citation will change accordingly.

KEY WORDS

Hyperspectral imaging, in vivo spectral imaging, spectral library, angiogenesis, radiometric imaging, melanoma, microvessel density

ACKNOWLEDGEMENTS

P.C.T. was supported by NIH Training Grant T32 NS043126-03. This work was supported by the National Cancer Institute's Network for Translational Research in Optical Imaging (NTROI) grant U54105008 (W.S.E-D.). J.M.L. is an Industrial Partner and Member of the NTROI Team at the University of Pennsylvania.

ABSTRACT

Molecular imaging techniques can detect and monitor characteristics of the tumor microenvironment, such as angiogenesis, hypoxia, metabolism, and apoptosis that may better correlate with response to cancer therapy and may provide information in real-time. We investigated the use of a novel, spatially discrete, hyperspectral, multi-fiber optical system to characterize selected regions of skin in living mice. We determined the reproducibility and robustness of the spectral signatures derived from comparable regions of interest. Additionally, we characterized spectral differences in vascular and non-vascular fields to determine their potential use in monitoring angiogenesis. The macroscopic Prism and Reflectance Imaging Spectroscopy System (MACRO-PARISS) was calibrated against a National Institute for Standards and Technology (NIST)-certified lamp, allowing for reproducible spectra with any instrument similarly calibrated. Spectra were classified using a linearity-independent algorithm over a wavelength range of 450-920 nm. Classified spectra were integrated into a spectral library and subsequent acquisitions were correlated with the library set to a minimum correlation coefficient (MCC) of 99%. The results indicated that similar regions of interest with respect to vascularity consistently generated a unique spectral signature. As the field of view (FOV) moved from vascular to non-vascular areas, the acquired spectra changed in a step-wise and predictable fashion. Additionally, vascular fields that were deprived of their blood supply subsequently generated a non-vascular spectral signature. This work has implications for the monitoring of various physiologic or pathological processes including tumor angiogenesis and the therapeutic effects of anti-vascular agents.

INTRODUCTION

Traditional medical imaging modalities such as computed tomography and magnetic resonance imaging have significantly advanced our understanding of cancer behavior and have provided a means for objectively determining tumor response to anticancer therapeutics. Previous historical definitions of tumor response such as the WHO criteria,[1] varied greatly among researchers, creating a serious challenge in reporting results in a consistent manner. In an attempt to address these limitations, an international collaboration of academicians, industry representatives, and regulatory authorities established a unified, international standard for tumor response assessment in 2000, termed the Response Evaluation Criteria in Solid Tumors (RECIST), that was based on CT and MRI linear measurements of lesion size.[2]

Recently, the National Cancer Institute (NCI) has called for the improvement of the RECIST methodology since these anatomical imaging techniques have proved to be less than optimal predictors of therapeutic response[3] in comparison to the detection of molecular events that may better correlate with diagnosis, staging, prognosis and response to cancer therapy.[4] Tumor microenvironment characteristics including angiogenesis, hypoxia, apoptosis, and tumor cell metabolism are believed to dictate tumor behavior and precede morphological end-stage phenomena. Molecular imaging methods using optical, PET, or SPECT hold promise for detecting changes in the tumor microenvironment manifesting shortly after therapy, in detecting cancers earlier, and in providing functional information that can greatly influence the physician's therapeutic approach.

Hyperspectral imaging (HSI) is a form of optical imaging that is used by the Remote Earth Sensing Community for environmental studies, and is typically used in radiometric mode. HSI can detect the location of spectral objects such as soil composition, minerals, coastal zone oceanic regions, and vegetation. An HSI instrument can be broadly defined as any instrument that faithfully digitizes an analog spectrum presented by the field of view (FOV). This requires that each spectrum be characterized by a large number of data

points that in the case of a spectrometer means high spectral resolution (better than 5 nm).

This concept of characterizing and diagnosing unique spectral signatures from a remote distance on a heterogeneous complex FOV has recently been applied to histological tissue slides[5] and in live mice,[6-8] providing spectral data that complements traditional morphological characterization.

With a pressing need to develop imaging techniques that may better assess tumor response at the molecular level, we investigated whether a prototype hyperspectral imaging fiber-optic probe could generate reproducible and unique spectral signatures (dominantly scattered from within the tissue) when imaging cutaneous vascular and non-vascular regions in living mice. Our interest is in the eventual development of this technology in assessing tumor microenvironment processes, including angiogenesis. The induction of new blood vessel formation is a prominent feature of solid tumors and it is well established that tumor size beyond 2 mm^3 requires the construction of a vessel network.[9,10] Mean vascular density has been correlated to progression of cutaneous melanoma[11,12] and a number of histopathological studies have reported a correlation between overall survival in melanoma patients and tumor microvessel density,[13-16] supporting the notion of a vascular density gradient and vertical tumor progression.

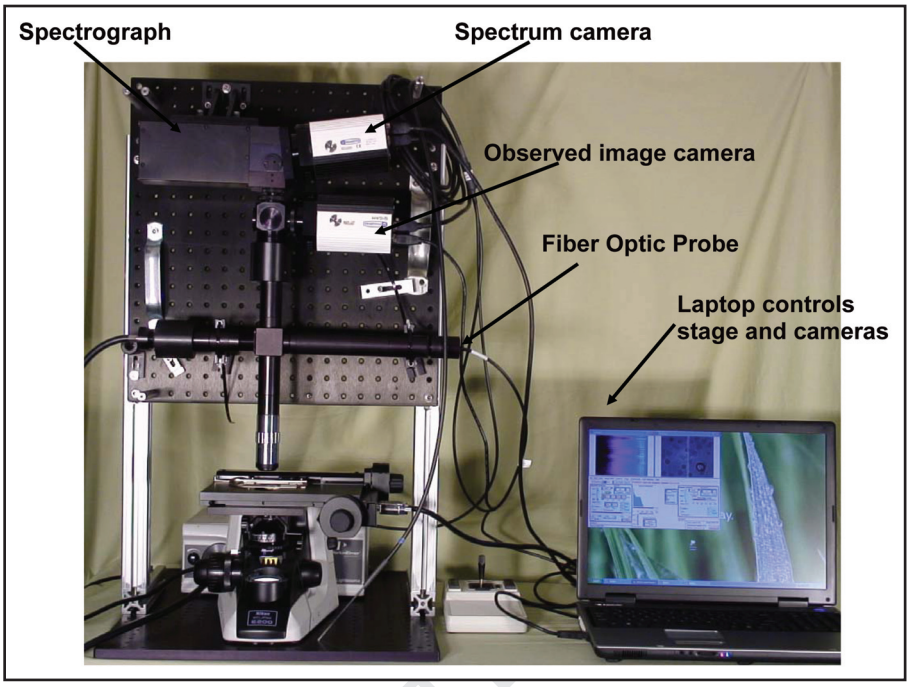

Figure 1. A photograph of the prototype in vivo MACRO-PARISS hyperspectral imaging system. Arrows indicate the fiber-optic imaging probe, an imaging spectrometer, a QICAM camera, an observed image camera, and laptop that controls the cameras (High intensity tungsten halogen lamp not shown).

We hypothesized that our prototype HSI system could generate quantifiable spectral differences in a reproducible manner between vascular and non-vascular regions of skin. The HSI system used in these experiments incorporated a high intensity tungsten halogen lamp coupled with a PARISS (Prism and Reflector Imaging Spectroscopy System)-based customized remote fiber-optic imaging probe. The high intensity tungsten lamp was used as the source of light because it provided a greater amount of red intensity, ideal for penetrating and probing living tissues. Additionally, since many variables within an in vivo skin section such as pH, protein interactions, temperature, and ionic concentration preclude a linear mixture of spectral colors, the PARISS system was suitable for this evaluation due to its ability to process non-linear high resolution spectral data. Spectral images were generated using a charge-coupled device (CCD) detector and the spectrometer was calibrated against an ion-discharge wavelength calibration lamp.

We generated spectral data from living mice and analyzed vascular and non-vascular skin regions to provide insight into the utility of this prototype HSI fiber-optic system. The results of this study support the notion that this system can reproducibly differentiate highly vascular tissue from less vascular tissue. Further investigations of this HSI system could be done to monitor angiogenic changes within a tumor microenvironment before and after therapeutic interventions.

MATERIALS AND METHODS

Hyperspectral imaging system instrumentation. The in vivo hyperspectral imaging system consists of a spatially discrete, multi-fiber optic imaging probe (LightForm, Inc., Hillsborough, NJ), an imaging spectrometer integrated with a QICAM camera (Q Imaging, Burnaby Canada), and a second QICAM acting as an observed image camera (Fig. 1).

The fiber-optic probe consists of 17 illumination fibers and 18 signal collection fibers, randomly distributed, with each fiber having a 50-micron core. Signal collection fibers were arrayed along a slit and imaged onto the PARISS entrance slit. Each fiber delivered spectral information from a different point in the FOV.

The MACRO-PARISS system (LightForm, Inc., Hillsborough, NJ) is a prism based imaging spectrometer that originated within the remote Earth sensing community. This system was chosen because of its very high light transmission (>90%) characteristics typical of prism systems. The imaging spectrometer portion operates in spectrograph configuration in which all wavelengths between 365 and 920 nm are presented simultaneously. Acquiring all wavelengths within a single fast acquisition accommodates movement in the FOV without affecting the integrity of a spectral acquisition. In this study, we chose a range of 450 to 920 nm.[17]

Calibration, normalization and validation. The MACRO-PARISS spectrometer was first wavelength calibrated using a multi-ion discharge lamp (MIDL), (LightForm, Inc., Hillsborough, NJ) that emits Hg+, Ar+ and inorganic fluorophores (Fig. 2). Each pixel in a column of the spectrum CCD corresponds to a specific wavelength. The MIDL lamp provides the absolute wavelength information provided by the ion emission lines. The MACRO-PARISS software provides an algorithm that matches the spectral features to pixel with subsequent calibration of the entire spectrometer. The wavelength accuracy was validated to be better than 0.5 nm over the entire spectral range.

Spectral resolution was confirmed by measuring the number of pixels that covered the full width at half maximum (FWHM) at the 436 nm Hg line. The wavelength spread at FWHM was determined to be 1.2 nm +/- 0.25 nm.

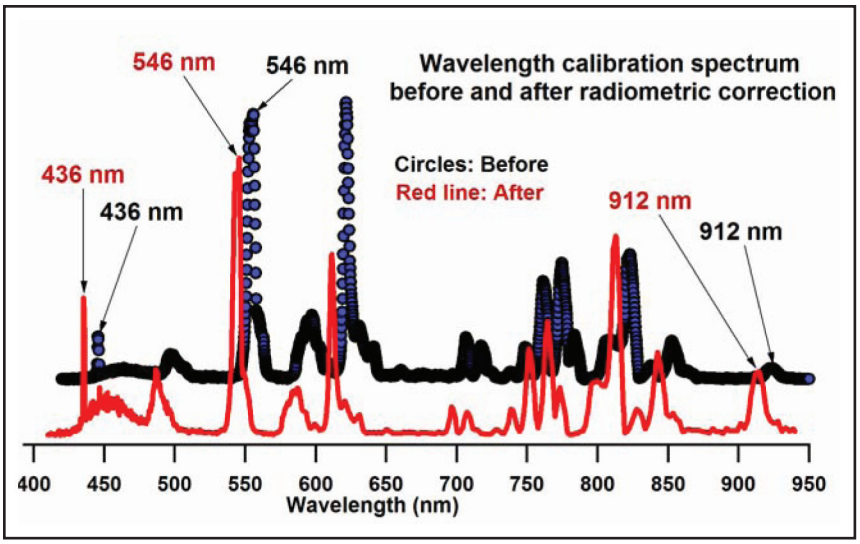

Figure 2. The solid line shows the MIDL wavelength calibration lamp spectrum after normalization, and the dotted line before normalization. Note that following normalization, the spectral range around 436 nm and 900 nm increased in intensity, and the 546 nm line was almost unchanged.

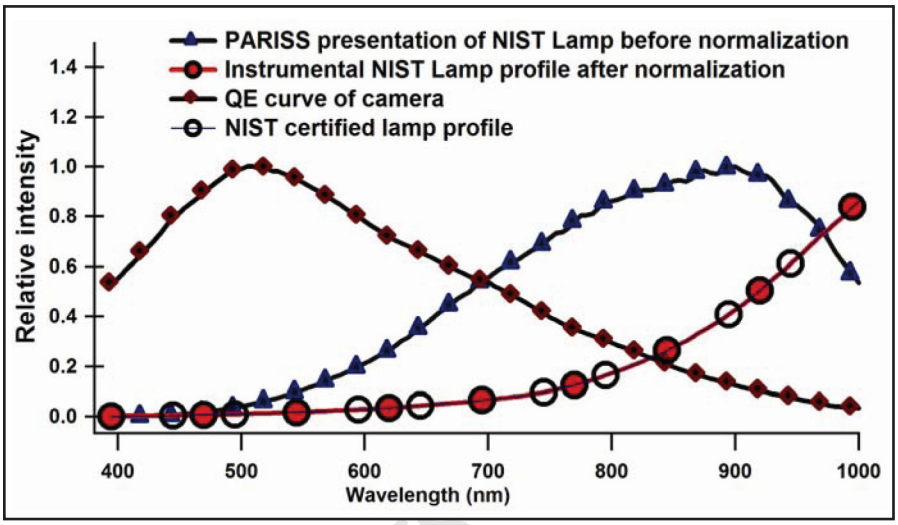

Figure 3. The line with red diamond markers shows the QE profile of the camera. The line with blue diamonds presents the profile as rendered by the MACRO-PARISS system and is a convolution of the QE of the camera, the actual spectral profile of the lamp, coatings, fiber optic, and all other optical elements. The curve with open circles is the profile in the NIST-certified profile; and the superimposed curve with solid circles is the normalized MACRO-PARISS profile of the lamp following normalization.

The MACRO-PARISS spectrometer was then normalized to remove instrumental contributions due to the Quantum Efficiency (QE) of the camera, coatings on lenses, the fiber-optic and prism transmission properties, and reflectivity of mirrors in the system. A NIST-certified halogen lamp (NCHL) (Model LS-1-Cal, Cert #1013, Ocean Optics, Inc, Dunedin FL) was used that was supplied with a spectral profile in ASCII listing wavelength versus power ($\mu W/cm^2/nm$). This is the profile any radiometric spectrometer would report when characterizing this lamp. The MACRO-PARISS software incorporates the algorithm to enable this normalization. Figures 2 and 3 show the profile of the NCHL reported by the MACRO-PARISS spectrometer before and after correction, and the QE of the camera. The corrected profile is seen to be a perfect match to the profile shown on the lamp's certificate.

Light source, calibration and methods. A high intensity tungsten halogen lamp set to the highest brightness was used as the light source for the fiber-optic probe to increase signal-to-noise data at the ends of the spectral range and for greater red intensity. The wavelength range from 450 to 920 nm, especially in the near IR, above 650 nm, experiences less absorption in living tissues and would theoretically provide valuable tissue spectral information otherwise not accounted for with other light sources.

The entire spectral system, including the probe, was wavelength-calibrated daily prior to imaging experiments to ensure accuracy using the MIDL emission source as described above. Spectral sensitivity was checked in the advanced display mode with amplitude plotted against wavelength at the time of calibration. After wavelength calibration, the system was normalized radiometrically through the fiber-optic probe with the NIST certified, halogen light source. A correction curve was then generated in the MACRO-PARISS software to correct all acquisitions to the standard.

Since each fiber in the bundle presents light to the MACRO-PARISS slit according to its respective location in the FOV, we attempted to account for a heterogeneous FOV by using a fiber-optic probe with a relatively higher number of individual fibers as described in the instrumentation section. This would provide spatial information and allow us to characterize field heterogeneity. The fact that we deliver in vivo spatial information differentiates our system from traditional spectral modalities that acquire a single, homogenized, all encompassing, data-point.[18-20]

Additionally, we recognize, and are currently addressing, the ability to map the 18 collection fibers to the slit in order to generate a low resolution graphic image. We could then determine the location and amplitude of signal from every point in the FOV of the probe, generating a hyperspectral data cube consisting of wavelength, spatial and graphic information.

In vivo spectral acquisition and acquisition parameters. The branching artery of the SCID mouse ear was used as our model because it has adjacent regions of vascular and non-vascular skin. Nude mice were selected because their ears have a consistent vascular anatomy, allowing for a clear comparative analysis between vascular and non-vascular acquisitions. Additionally, we anticipated that hair would contribute to a spectral signature and hence, nude mice would circumvent this issue for these experiments.

Using an Institutional Animal Care and Use Committee (IACUC)-approved protocol, three nude mice were anesthetized with a ketamine/xylazine solution (125 mg/kg and 15 mg/kg, respectively) via intraperitoneal injection. Subsequently, the probe was gently placed with uniform pressure on the skin, ninety degrees to the selected region for spectral acquisition.

Parameters to reduce single acquisition variability. Specific acquisition parameters were determined based on an inverse relationship between movement variability of the user and

acquisition variability. The fact that all wavelengths were acquired simultaneously ensured that there was no variability from wavelength to wavelength; however, movement of the probe due to the user could result in differences in the illuminated area. The greater the acquisition times the lesser the acquisition variability but the greater the chance of movement by the user.

We attempted to address the problem of spectral sampling variability by using standard analytical sampling procedures. Each in vivo skin acquisition consisted of five co-added 25 millisecond acquisitions five times; resulting in an improvement in signal-to-noise ratio (S/N) of a factor of 2.2 (square root of 5). Each area was sampled five times. We found that this was an optimal balance where any investigator could hold still, without compromising the acquisition quality and hence, maintain a well-defined S/N ratio.

A total of nine distinct skin regions (Areas 1-9) were imaged in triplicate on different days and subsequently compared (Fig. 4). At the time of sacrifice, vascular and non-vascular skin areas were imaged before and after stripping the vascular blood supply to the ear via a 1 cm surgical incision made at the base of the ear, with subsequent drainage of the blood to gravity.

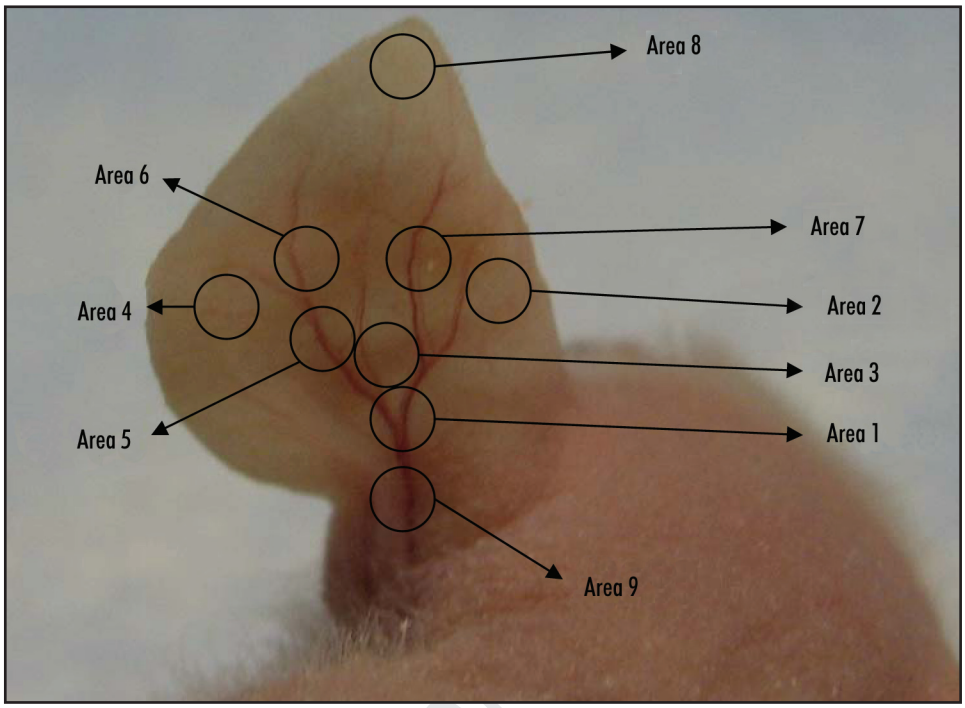

Figure 4. A photograph of the 9 areas designated for hyperspectral imaging. Note the clear juxtaposition of vascular and non-vascular areas. This consistent vascular anatomy allowed for analysis of inter- and intra-animal imaging variability of generated spectral data. Acquiring images of the same area on different mice as well as imaging the same area on the same mouse but on different days was possible.

Image analysis software. We assumed that many physiologic variables within an in vivo skin region would preclude a linear mixture of spectral signatures. The MACRO-PARISS system accounts for this physiological challenge since it is able to process non-linear spectral data from spectral objects localized near each other. Master spectral libraries (MSL) were generated from acquired spectral data through a supervised classification using a spectral waveform cross correlation analysis (SWCCA) algorithm. All library spectra were saved in radiometric format (Fig. 5A). Spectra corresponding to more vascular areas were pseudo-colored in redder colors and non-vascular areas in bluer colors. Note that a minimum was formed around 550 nm that probably corresponds to absorption by red blood cells.

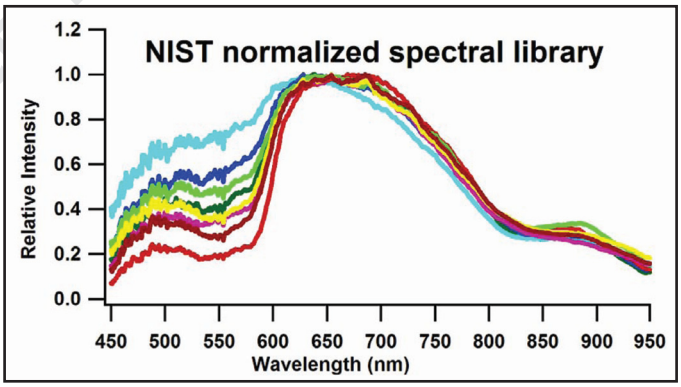

Figure 5A. Radiometric Master Spectral Library (MSL). Light colors tend towards areas in the FOV without vasculature and those in redder colors indicate the presence of blood vessels.

While previous studies have used a combination of automated and supervised classification schema for generating MSL, we took a more conservative strategy since an automated classification would have included spectral data from the peripheral regions of the fiber-optic collection fibers, leading to less robust spectral signatures. Each spectrum that was manually added to the MSL was designated a pseudo color. All spectra from the original FOV were then correlated with the MSL, set to a minimum correlation coefficient (MCC) of 99%. Only when the spectrum from the FOV correlated at 99% or greater with an MSL spectrum, did the pseudo-color replace the gray scale pixel. Additionally, histograms of MSL pseudo-color members were generated to present spectral ratios within the FOV and were used to compare vascular and non-vascular skin regions.

RESULTS

Reproducibility and robustness of acquired MACRO hyperspectral signatures. Our approach to testing the reproducibility of the MACRO-HSI system consisted of imaging the vascular anatomy of the ear, since it allowed us to image the same designated areas on the same mouse on different days, as well as between mice. This approach would allow us to assess intra- and inter- animal imaging variability. All four areas of the ear were imaged in triplicate on different days.

The Master Spectral Library (MSL) was used to generate all ear spectral histograms. All spectra from the original FOV were correlated with the MSL, set to a minimum correlation coefficient (MCC) of 99%. We manually added spectra from the spectral image from light captured exclusively from the center (core) of the 18 collection fibers. This served to create a more robust spectral library since it did not include spectral data from the walls of the collection fibers. Each fiber delivered a spectral signature from a different point on the FOV.

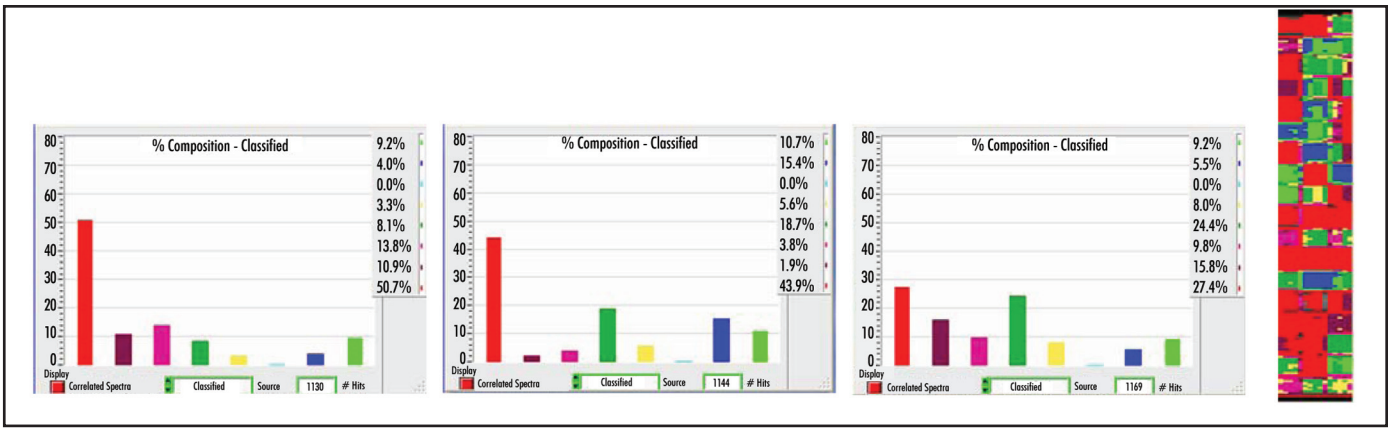

Figure 5B. Using a MCC of 99%, spectral histograms depicting percent composition of spectral objects were generated from Area 1 (vascular). The components of the histogram are a result of our ability to display and characterize spatial heterogeneity. Images were acquired on three separate days on the same mouse. The spectral image to the far right represents the same spectral data in spectral format. Note the consistency in spectral signatures in histogram and spectral format, supporting the notion that this HSI system can generate reproducible signatures over comparable regions of interest. Spectral histograms for all nine areas were similarly generated for analysis.

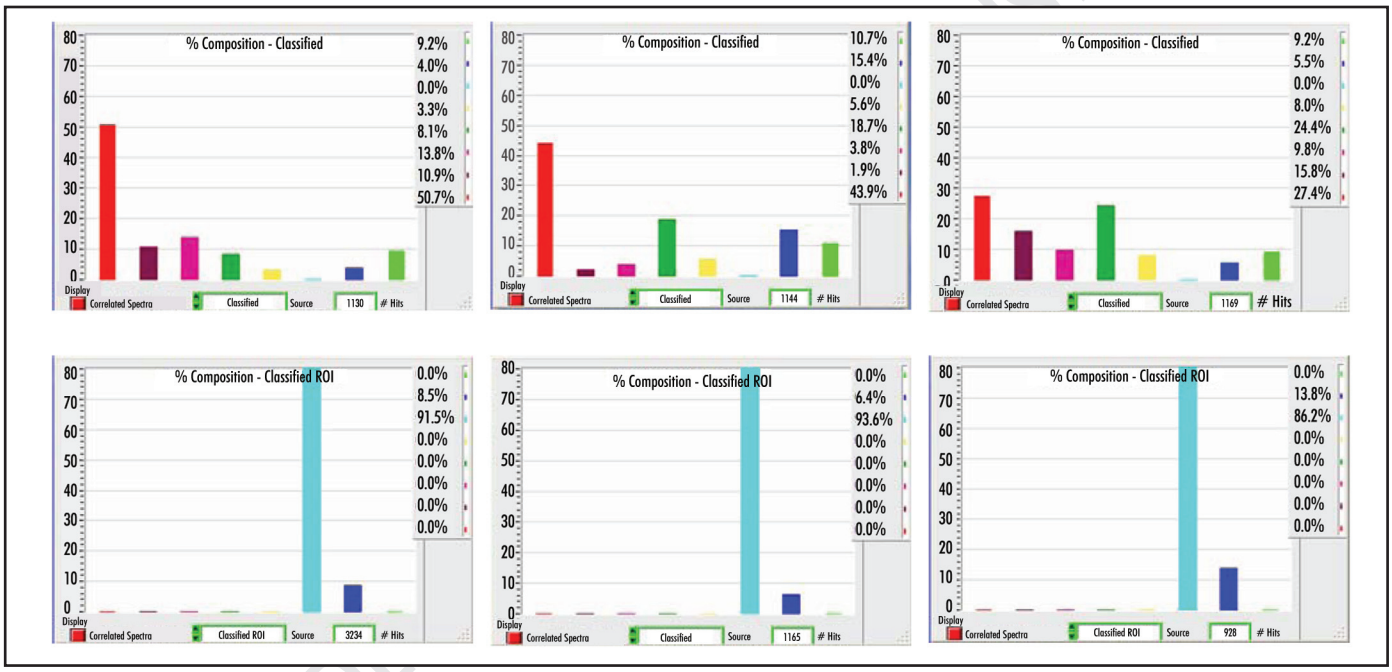

Figure 6. Spectral histograms of Area 1 (top row-vascular) and Area 4 (bottom row-non vascular). Note the spectral differences in vascular regions of the skin when compared to non-vascular regions. All spectral histograms were generated from an MSL at 99% MCC.

Figure 5B clearly demonstrates the consistency in spectral histograms generated from the nine areas of variable vascularity within the mouse ear.

In vivo hyperspectral differentiation of vascular and non-vascular regions of the SCID mouse ear. We compared spectral histograms of vascular and non-vascular regions of the skin. Figure 6 illustrates the spectral differences in vascular regions (Areas 1 and 3) of the skin as compared to non-vascular regions (Areas 2 and 4). The results indicate that similar regions of interest with respect to vascularity consistently generated a unique spectral signature. We further characterized the uniqueness of the vascular spectral signature by imaging additional regions of the ear, Areas 5-9. These additional areas were chosen for analysis because they all included visible vascularity but differed with respect to the level of gravity pull and their distance from the base vascular supply. We sought to image a gradation of vascular prominence as a potential surrogate marker for vessel formation and retraction.

With these additional areas, we hypothesized that Areas 5 and 9 would generate spectral signatures similar to 1 and 3 (i.e., a vascular signature) while Area 8 would closely resemble Areas 2 and 4 (i.e., a non-vascular signature). Areas 6 and 7 might behave in one of two ways: either 1) these areas would capture a signature that would be a combination of vascular and non-vascular signatures or 2) capture a vascular signature.

The results confirmed our hypothesis that the spectral histograms of Areas 5 and 9 closely resembled Areas 1 and 3. We additionally found that Areas 6 and 7 displayed a "hybrid" spectral histogram between that of Areas 5, 9 and Area 8 (Fig. 7). This data led to the characterization of a unique vascular signature.

Overall, these findings led to our conclusion that the SCID

mouse ear may provide a model to establish a vascular hyperspectral signature spectrum as one moves away from the base of the ear, against gravity, towards to apex of the ear. This data also supports the conclusion that the MACRO-PARISS HSI system fiber-optic attachment provides reproducible vascular and non-vascular signatures. As the FOV moved from vascular to non-vascular areas, the acquired spectra changed in a step-wise predictable fashion.

Removal the blood supply from a vascular field with subsequent spectral acquisitions. At the time of mouse sacrifice, vascular and non-vascular skin regions were imaged before and after stripping the vascular blood supply to the ear via a 1 cm surgical incision made at the base of the ear with subsequent drainage of the blood with gravity. We hypothesized that removal of the blood supply would lead to vascular regions taking on a new non-vascular spectral signature. Additionally, we expected no change in spectral signatures in regions that were non-vascular prior to stripping the vascular blood supply. Figure 8 illustrates vascular regions taking on non-vascular spectral signatures after the removal of their blood supply. This approach further supports the conclusion that the spectral signatures are indeed vascular and non-vascular.

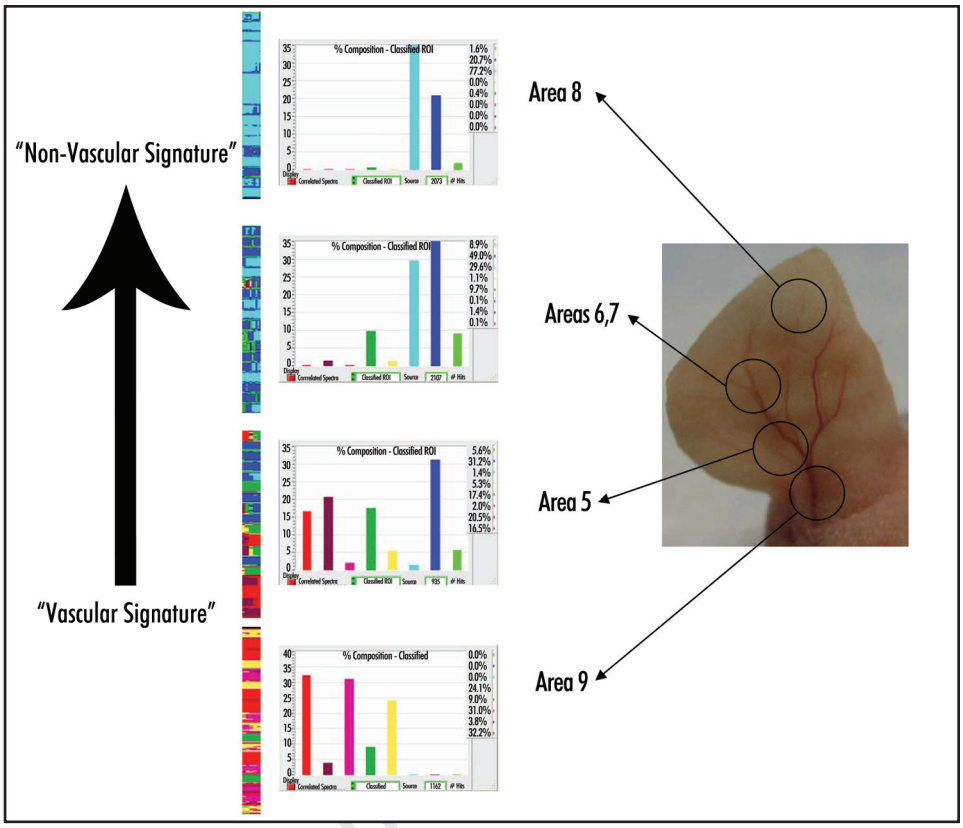

Figure 7. Spectral histograms of Areas 5 and 9 closely resembled a vascular signature. Note the "hybrid" spectral histogram displayed in Areas 6 and 7. Spectral images are displayed next to their respective histogram. Movement of the probe from a vascular to a non-vascular area results in a significant and step-wise change in spectral signatures.

DISCUSSION

We investigated the use of the MACRO-PARISS system, a novel spatially-discrete hyperspectral multi-fiber optical system to characterize vascular and non-vascular regions of skin in living mice. Establishing use of this system in discriminating vascular and non-vascular areas could allow assessment of physiologic and pathologic processes in the tumor microenvironment. Utilizing this MACRO-PARISS system coupled to a remote fiber-optic imaging probe, we established the reproducibility and robustness of the spectral signatures derived from comparable regions of interest.

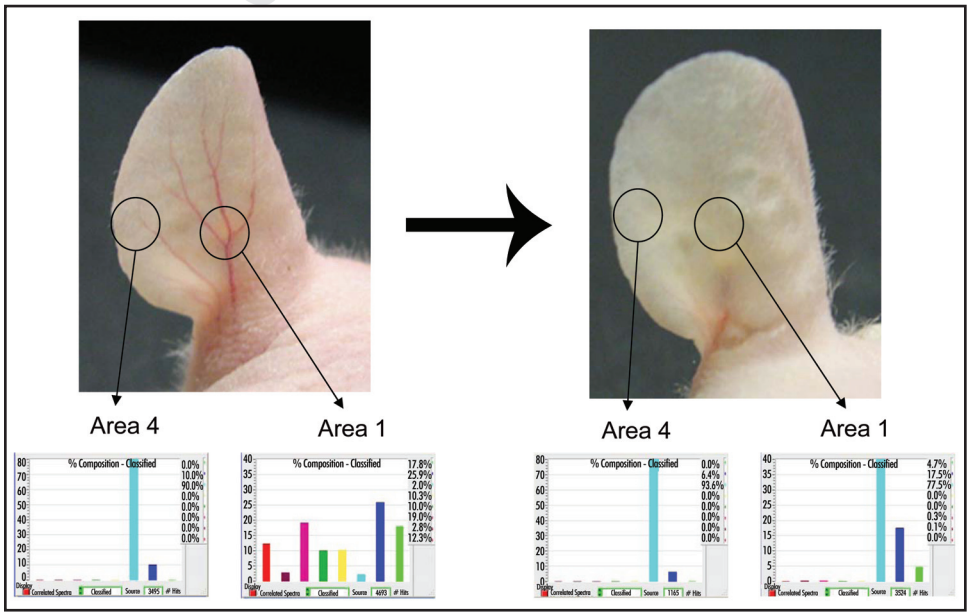

Figure 8. Reversion of a vascular spectral signature (Area 1) to a non-vascular spectral signature after the removal of its blood supply. Area 4 did not change before and after the removal of the blood supply. All spectral histograms are composites of triplicate imaging acquisitions.

Performance optimization of the HSI system in generating reproducible and unique spectral signatures was determined by three main factors. First, we used a high intensity tungsten lamp as a light source, which allowed the emission of light in the red range, and hence, experiences less absorption by tissue. Additionally, we set appropriate acquisition parameters that increased the S/N ratio and reduced single acquisition variability. In regards to creating the MSL, we manually placed spectra that only came from the center of the signal collection fibers, leading to a more robust MSL.

Based on the vascular anatomy of the SCID mouse ear, we identified a unique vascular spectral signature. Regions that generated vascular spectral signatures changed their signature when the vascular supply was removed, further supporting the robustness of this

signature. Additionally, we showed that a vascular signature spectrum exists as one moves from vascular to non-vascular regions, and these changes occur in a step-wise and predictable fashion.

With these experiments demonstrating a gradual spectral signature change in a predictable fashion based on the relevant regional presence of vascularity, we concluded that this MACRO-PARISS HSI system might provide a capability to monitor subtle changes in tumor vascularity before and after therapeutic intervention. We recognize that optical imaging techniques have depth of penetration limitations based on absorption, reflection, and scatter; however, there is a clear potential application to cutaneous inflammatory and cancerous lesions, gastrointestinal lesions via colonoscopy and/or esophagoscopy, and during surgery such as in lymph node assessment. Additionally, the system has potential in differentiating oxy- and deoxyhemoglobin as a surrogate marker of tumor hypoxia. In the future it may be possible to translate this method of data acquisition to the clinic as a reliable adjunct to the pathologist, oncologist, surgeon and dermatologist in monitoring tumor response after therapeutic intervention.

References

1. World Health Organization. WHO Handbook for Reporting Results of Cancer Treatment. Geneva: World Health Organization, 1979.
2. Therasse P, et al. New guidelines to evaluate the response to treatment in solid tumors: European organization for research and treatment of cancer, national cancer institute of the united states, national cancer institute of canada. J Natl Cancer Inst 2000; 92:205-16.
3. Czernin J, Weber WA, Herschman HR. Molecular imaging in the development of cancer therapeutics. Annu Rev Med 2006; 57:99-118.
4. Kelloff GJ, et al. The progress and promise of molecular imaging probes in oncologic drug development. Clin Cancer Res 2005; 11:7967-85.
5. Dicker DT, et al. Differentiation of normal skin and melanoma using high resolution hyperspectral imaging. Cancer Biol Ther 2006; 5:1033-8.
6. Martin ME, et al. Development of an advanced hyperspectral imaging (HSI) system with applications for cancer detection. Annals of Biomedical Engineering 2006; 34:1061-8.
7. Zavattini G, et al. A hyperspectral fluorescence system for 3D in vivo optical imaging. Physics in Medicine and Biology 2006; 51:2029-43.
8. Chaudhari AJ, et al. Hyperspectral and multispectral bioluminescence optical tomography for small animal imaging. Physics in Medicine and Biology 2005; 50:5421-41.
9. Boehm T, Folkman J, Browder T, O'Reilly MS. Antiangiogenic therapy of experimental cancer does not induce acquired drug resistance. Nature 1997; 390:404-7.
10. Folkman J. What is the evidence that tumors are angiogenesis dependent? J Natl Cancer Inst 1990; 82:4-6.
11. Marcoval J, et al. Angiogenesis and malignant melanoma: Angiogenesis is related to the development of vertical (tumorigenic) growth phase. J Cutan Pathol 1997; 24:212-8.
12. Erhard H, et al. Transition of horizontal to vertical growth phase melanoma is accompanied by induction of vascular endothelial growth factor expression and angiogenesis. Melanoma Res 1997; 7(Suppl 2):S19-26.
13. Srivastava A, Laidler P, Davies RP, Horgan K, Hughes LE. The prognostic significance of tumor vascularity in intermediate-thickness (0.76-4.0 mm thick) skin melanoma: A quantitative histologic study. Am J Pathol 1988; 133:419-23.
14. Straume O, Salvesen HB, Akslen LA. Angiogenesis is prognostically important in vertical growth phase melanomas. Int J Oncol 1999; 15:595-9.
15. Vlaykova T, et al. Prognostic value of tumour vascularity in metastatic melanoma and association of blood vessel density with vascular endothelial growth factor expression. **Melanoma** Res 1999; 9:59-68.
16. Kashani-Sabet M, Sagebiel RW, Ferreira CM, Nosrati M, Miller IIIrd JR. **Tumor vascu**larity in the prognostic assessment of primary cutaneous melanoma. J Clin Oncol 2002; 20:1826-31.
17. Lerner JM. Imaging spectrometer fundamentals for researchers in the biosciences-a tutorial. Cytometry 2006; A69:712-34.
18. Yodh AG, Boas DA. Functional imaging with diffusing light. In: Vo-Dinh T, ed. Boca Raton: CRC Press, 2003.
19. Yodh A, Chance B. Spectroscopy and imaging with diffusing light. Physics Today 1995; 34-40.
20. Angelopoulou E. Understanding the color of human skin. Proceedings of the SPIE Conference on Human Vision and Electronic Imaging 2001; VI4299:243-51.